

This document is the Accepted Manuscript version of a Published Work that appeared in final form in ACS Catalysis, copyright © American Chemical Society after peer review and technical editing by the publisher. To access the final edited and published work see <https://pubs.acs.org/doi/abs/10.1021/acscatal.7b01415>.

A Generalized Picture of C-C Cross-Coupling

Michael Busch,^{1,a} Matthew D. Wodrich,² and Clémence Corminboeuf^{2*}

¹Laboratory for Computational Molecular Design and National Center for Computational Design and Discovery of Novel Materials (MARVEL), Ecole Polytechnique Fédérale de Lausanne (EPFL), 1015 Lausanne, Switzerland

²Laboratory for Computational Molecular Design, Institute of Chemical Sciences and Engineering, Ecole Polytechnique Fédérale de Lausanne (EPFL), 1015 Lausanne, Switzerland

email: clemence.corminboeuf@epfl.ch

Abstract: Transition metal catalyzed cross-coupling reactions occupy a privileged position in chemistry because of their ability to link myriad functional groups. The numerous variants of this class of reactions (*e.g.*, Suzuki, Kumada, Negishi, etc.) differ in the transmetallation agent used to transfer “R” groups onto the catalyst. While understanding any single variant (*e.g.*, Suzuki coupling) can be accomplished through direct analysis of the catalytic cycle, a comprehensive picture that illustrates the interrelationships between the different types of cross-coupling reactions remains absent. Here, using a tool built upon a three-dimensional volcano plot we create a generalized thermodynamic picture of C-C cross-coupling reactions. This “cross-coupling” genome not only facilitates better understanding of catalytic behavior, but also outlines strategies for developing new reaction protocols through the manipulation of easily computed descriptor variables.

Keywords: Cross-coupling, Volcano Plot, Linear Scaling Relationships, Homogeneous Catalysis, Density Functional Theory

^a Current Address: Department of Physics, Chalmers University of Technology, Fysikgränd 3, SE-412 96 Göteborg, Sweden.

This document is the Accepted Manuscript version of a Published Work that appeared in final form in ACS Catalysis, copyright © American Chemical Society after peer review and technical editing by the publisher. To access the final edited and published work see <https://pubs.acs.org/doi/abs/10.1021/acscatal.7b01415>.

Introduction

The formation of new C-C bonds via cross-coupling reactions represents a key weapon in the arsenal of today's synthetic chemist. The versatility and importance of these reaction types cannot be overstated, as attested to by the considerable number of books,¹⁻⁴ review articles,⁵⁻⁹ and, of course, the awarding of the 2010 Nobel Prize in Chemistry to Heck, Negishi, and Suzuki for "palladium-catalyzed cross couplings in organic synthesis."¹⁰⁻¹² Numerous varieties of cross-coupling reaction exist, each with individual strengths and weaknesses (*e.g.*, different functional group tolerances, etc.). One overarching constant, however, is the need for a transition metal based catalyst that facilitates creation of the final products. As indicated in their Nobel citation, the seminal cross-coupling reactions of Suzuki,¹³⁻¹⁶ Negishi,¹⁷⁻¹⁹ and Heck²⁰⁻²² all employed Pd-based catalysts to expedite the desired chemical transformations. Other noteworthy cross-coupling "name" reactions employing Pd catalysts include those of Stille,²³⁻²⁶ Hiyama,²⁷⁻²⁹ and Kumada.³⁰⁻³² The breadth of modern cross-coupling protocols has expanded considerably since those pioneering works,^{13,17,23-25,27,30,31,33,34} including the development of new cross-coupling partners (*e.g.*, organolithium species),³⁵ a proliferation in the use of catalysts incorporating earth abundant metal centers (*e.g.*, Fe or Ni),³⁶⁻⁴⁹ as well as new ligand systems.⁵⁰⁻⁵⁹ Despite noteworthy progress in identifying cheaper and more environmentally responsible catalysts, considerable work remains to further improve the activity and functional group tolerance of these new species. To accomplish this objective, it is desirable to enhance understanding of not only the individual factors that influence catalytic activity but also their relationship to one another, such that new reaction protocols can be rationally designed.

Pinpointing new catalysts possessing one or more desired properties can be accomplished in myriad ways, with different communities having their preferred methods. In heterogeneous and electrochemical catalysis, for example, the search for new species often

This document is the Accepted Manuscript version of a Published Work that appeared in final form in ACS Catalysis, copyright © American Chemical Society after peer review and technical editing by the publisher. To access the final edited and published work see <https://pubs.acs.org/doi/abs/10.1021/acscatal.7b01415>.

employ volcano plots,^{60,61} which permit facile comparison of large numbers of potential candidates in terms of, *e.g.*, turn-over frequency, overpotential, or desirable thermodynamics.⁶²⁻⁶⁴ Catalysts with appealing characteristics appear high (*e.g.*, near the peak or on the plateau) on a volcano plot, while those catalysts with worse profiles appear lower. The volcano plot's intuitive nature greatly enables the facile identification of catalysts possessing high activity. Recently, we transferred this highly valuable tool from heterogeneous/electro-catalysis into the realm of homogeneous catalysis,^{65,66} and showed that volcano plots successfully reproduced a host of experimental observations. Naturally, differences do exist between heterogeneous, electrochemical and homogeneous catalytic systems. For the former, volcano plots are normally cast in a strictly thermodynamic picture, where only reactants, intermediates, and products (and not the transition states connecting those species) found in the catalytic cycle are considered. Generally, the added complexity of homogeneous systems arising from factors such as stereoelectronics and steric bulk means that a thermodynamics only picture describes many, but not all aspects of the catalytic cycle. Indeed, the merits of considering a strictly thermodynamic as opposed to a combined thermodynamic/kinetic picture of the catalytic cycle has also been discussed by us in detail elsewhere.⁶⁶ Despite some shortcomings, volcano plots based only on thermodynamics for homogeneous processes still have the potential to yield general guidelines for predicting catalytic behavior. Thermodynamic volcano plots give a “best case scenario” for each catalyst and single out species that should be further scrutinized (*e.g.*, with a full computational analysis of the kinetics). Catalysts identified as being “poor” from these plots can be discarded as potential candidates, as even favorable kinetic profiles will be incapable of overcoming their thermodynamic deficiencies.

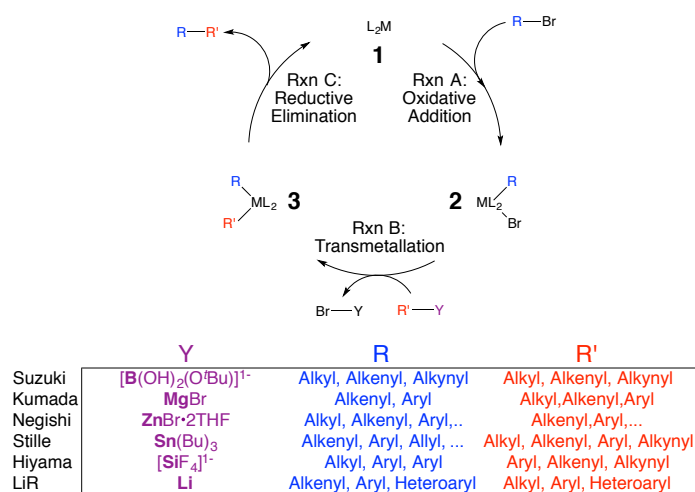


Figure 1. A generalized reaction mechanism, coupling partners (Y), and functional group tolerance (R/R') for various cross-coupling protocols. Note that Suzuki coupling uniquely involves a ligand exchange step in which Br is replaced by an alkoxy prior to transmetalation, which results in formation of a Y-alkoxy (as opposed to a Y-Br) species during Rxn B. This ligand exchange step is absent in the other cross-coupling protocols. Both the Suzuki and Hiyama coupling utilize activated coupling partners. Additionally, a recent study⁶⁷ has shown that the organozinc species used in Negishi coupling exist with tightly coordinated THF molecules, which have been included here.

While the ultimate success of a chemical transformation generally relies upon selecting an appropriate catalyst (perhaps identified via volcano plots), for homogeneous systems numerous other “external” factors might also be considered. This situation is perfectly illustrated by the different C-C cross-coupling protocols presented in Figure 1, which, despite employing similar (or identical) catalysts, tolerate and form new C-C bonds between different functional groups (R/R'=alkyl, aryl, alkenyl, etc.) with varying degrees of ease. For example, the choice of the coupling partner “Y” used during the transmetalation step (Rxn B, Figure 1) strongly influences the overall catalytic cycle energetics. Suzuki’s seminal work employed a palladium triphenylphosphine catalyst with an organoborate coupling partner (“Y” in Figure 1), which successfully coupled two vinyl groups (or a vinyl and an alkynyl) to form dienes (or enynes).¹³ However, the coupling partner “Y” can be changed, thereby creating different cross-coupling protocols. As such, the organoborate found in Suzuki coupling can be replaced by a Grignard reagent (the reaction is then known as Kumada coupling), which causes a corresponding change to the reaction’s energetic profile

This document is the Accepted Manuscript version of a Published Work that appeared in final form in ACS Catalysis, copyright © American Chemical Society after peer review and technical editing by the publisher. To access the final edited and published work see <https://pubs.acs.org/doi/abs/10.1021/acscatal.7b01415>.

(vide infra). Many other alterations are also possible, as shown in Figure 1 where a list of “name” and other cross-coupling reactions that utilize bromine and “classical” coupling partners (including activated species for Suzuki and Hiyama couplings) are given. While creating a comprehensive list of products desired by chemists undoubtedly necessitates multiple coupling strategies, one important missing element is a unified view that illustrates the thermodynamic interrelationship of the different cross-coupling protocols. The purpose of this contribution is twofold: (1) to create this generalized picture by developing a new 3-dimensional volcano plot^{68,69} and (2) to show ways to navigate within this plot in order to manipulate and optimize variables to achieve an ideal reaction. Here, in particular, we highlight the energetic influences of the cross-coupling partner for a prototypical cross-coupling reaction between two vinyl groups.

Methods

General Methods. Linear free energy scaling relationships and volcano plots were determined for the cross-coupling reaction of vinyl bromide and a vinyl metal complex using combinations of six metals (Ni, Pd, Pt, Cu, Ag, Au) and ligands taken from two different sets. The first set (Scheme 1, “Small Ligands”) consists of six small ligands that can rapidly be computed to establish linear free energy scaling relationships, but that are not normally used experimentally.⁷⁰ The second set (Scheme 1, “Realistic Ligands”) consists of bulkier phosphine, Buchwald, and N-heterocyclic carbene ligands (which are computationally much more expensive) but are more likely to be employed in an experimental setting. Our computations show that both sets produce nearly identical linear free energy scaling relationships (see Supporting Information Figures S1 and S2), which is an important point for future work where the objective is to quickly building new volcano plots to screen the viability of new catalysts. In this work, the cycles of 97 catalysts were computed in order to establish linear free energy scaling relationships and the resulting two- and three-dimensional volcano plots for the

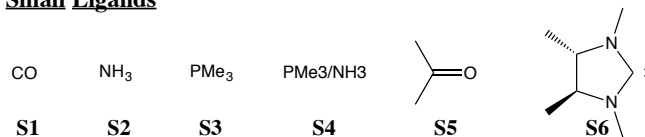
This document is the Accepted Manuscript version of a Published Work that appeared in final form in ACS Catalysis, copyright © American Chemical Society after peer review and technical editing by the publisher. To access the final edited and published work see <https://pubs.acs.org/doi/abs/10.1021/acscatal.7b01415>.

relevant cross-coupling reactions. The oxidation states of each catalyst were adjusted to align with the known 14e-/16e- nature of the coupling reactions, thus the coinage metal (Group 11) catalysts are treated as monocations. For the sake of establishing general trends, each catalyst was assumed to proceed through the catalytic cycle as a bisligated species⁷¹ [*i.e.*, with two (structure **1**) and four total ligand (structures **2** and **3**)] and with the R/Br and the R/R groups in the *trans* conformation for **2** and **3**, respectively. The theoretical catalytic reactions (both catalysts and transmetallation partners) were treated as single species infinitely diluted in implicit solvent. As a result of this treatment, issues surrounding the effects of ligand excess (including reaction inhibition⁷² and precipitation of the catalyst/metal⁷³) as well as the influence of aggregation of the transmetallation species are not considered here.

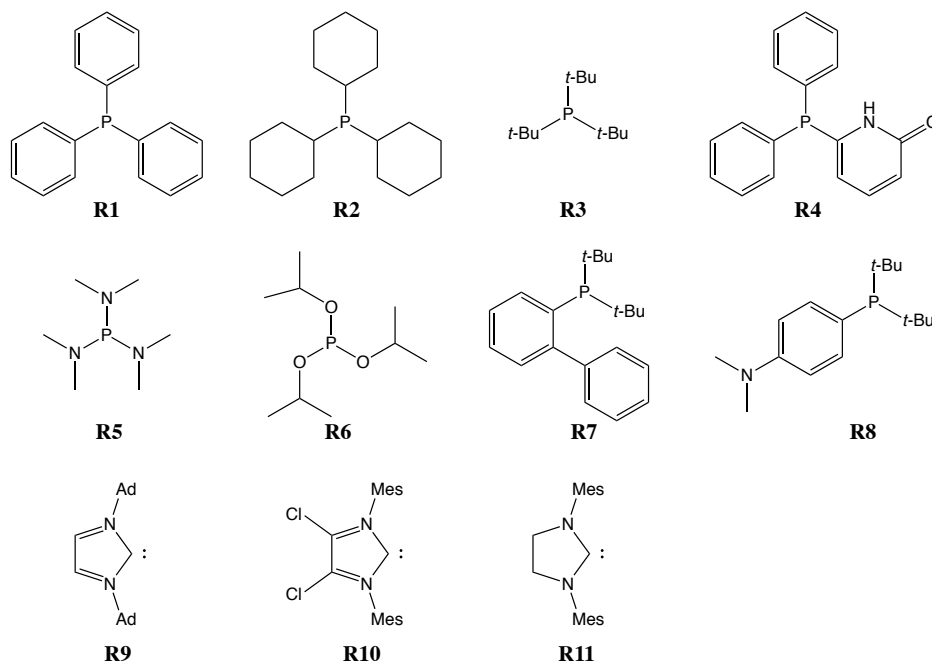
Scheme 1. Ligands used to establish linear free energy scaling relationships and to construct the volcano plots.

This document is the Accepted Manuscript version of a Published Work that appeared in final form in ACS Catalysis, copyright © American Chemical Society after peer review and technical editing by the publisher. To access the final edited and published work see <https://pubs.acs.org/doi/abs/10.1021/acscatal.7b01415>.

Small Ligands



Realistic Ligands



Computational Methods. The geometries of all species were optimized using the M06^{74,75} density functional coupled with the def2-SVP⁷⁶ basis set with solvation accounted for using the implicit SMD model⁷⁷ (in THF) as implemented in Gaussian09.⁷⁸ Known problems with the size of the integration grid⁷⁹ for the M06 functional were accounted for by using the “ultrafine” grid setting. Reported free energies include unscaled enthalpies and contributions arising from vibrational entropy only, as determined by vibrational analysis (see SI for further details). Scaling of the entropy contributions prevents the underestimation of association processes that occur within solvent (since the rotation and translation of molecules are strongly hindered) and has previously been employed to provide better energetic assessments of transition metal catalyzed reactions.⁸⁰⁻⁸³

Results and Discussion

This document is the Accepted Manuscript version of a Published Work that appeared in final form in ACS Catalysis, copyright © American Chemical Society after peer review and technical editing by the publisher. To access the final edited and published work see <https://pubs.acs.org/doi/abs/10.1021/acscatal.7b01415>.

Figure 1 illustrates the key mechanistic steps common to any cross-coupling catalytic cycle. In essence, the complete mechanism can be reduced to just three fundamental steps: oxidative addition, transmetalation, and reductive elimination.^{84,85} While this abbreviated mechanism remains virtually identical for each type of cross-coupling, energetic differences do arise when the coupling partner “Y” needed to complete the transmetalation step is changed (Figure 1).

Constructing volcano plots for each of the cross-coupling protocols listed in Figure 1 requires establishing linear free energy scaling relationships (LFESRs) between the catalytic cycle intermediates (see SI and ref.⁶⁵ for technical details and the mathematical derivations leading to the volcano plots). These LFESRs permit the relative energy of each stationary point on the potential energy surface to be estimated from the value of a “descriptor variable”. For our case, the suitable descriptor was previously shown to be the free energy associated with oxidative addition⁶⁵ (Figure 1, Rxn A), which also represents the magnitude of the binding interaction between the catalyst and the substrate and, thus, is a quantitative description of Sabatier’s principle.^{86,87} Sabatier’s principle states that an ideal catalyst should neither bind a substrate too strongly nor too weakly and that an optimal balance exists between adding reactants and dissociating products from the catalyst. Using the magnitude of this catalyst/substrate interaction as a descriptor, along with the associated LFESRs, it is possible to create a volcano plot that provides quantitative information concerning the free energies needed to complete different steps (*i.e.*, oxidative addition, transmetalation, reductive elimination) of the catalytic cycle. Note that we have previously discussed the construction of LFESRs and volcano plots in detail,^{65,66} and direct the interested reader to those references for more detailed explanations.

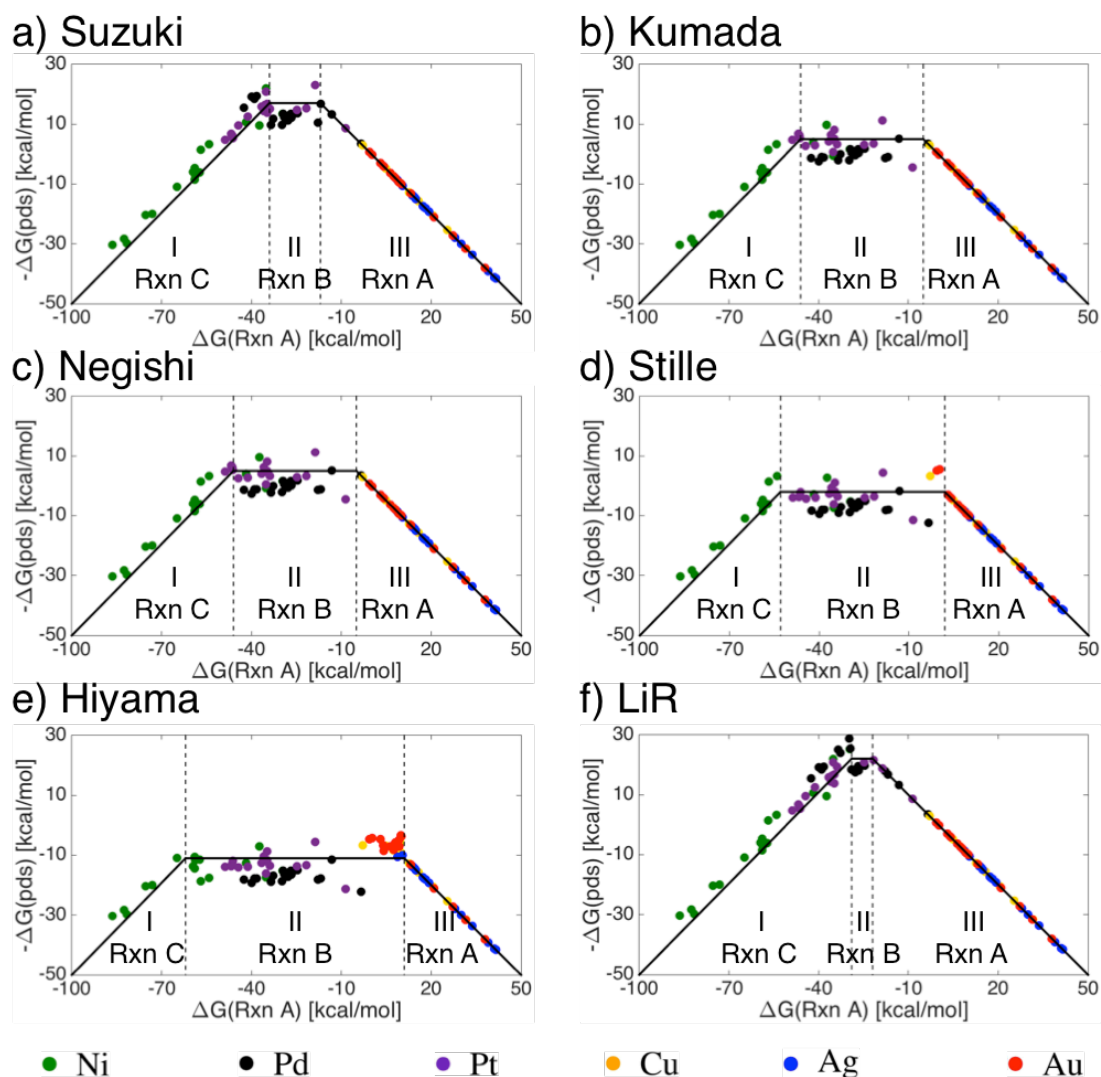


Figure 2. Volcano plots for several prototypical cross-coupling reactions: (a) Suzuki, (b) Kumada, (c) Negishi, (d) Stille, (e) Hiyama, and (f) LiR. Each plot is divided into three areas that define which catalytic cycle step is the most energetically costly (potential determining). In area I, reductive elimination (Rxn C) is the thermodynamically most difficult reaction step, while in areas II and III, transmetalation (Rxn B) and oxidative addition (Rxn A) are thermodynamically most difficult. Note that the y-axis plots the negative free energy of the potential determining step $[-\Delta G(\text{pds})]$. Thus, moving upward on the plot corresponds to catalysts having increasingly better thermodynamic profiles. See the supporting information for larger plots in which ligand/metal combinations are identified.

The volcano plots shown in Figure 2 were created by computationally analyzing a single reaction involving the coupling of vinyl bromide and a vinyl metal complex to form butadiene using 97 different catalysts (see methods section for details). Evaluating any of these volcano plots individually is relatively straightforward. The x-axis serves as the

This document is the Accepted Manuscript version of a Published Work that appeared in final form in ACS Catalysis, copyright © American Chemical Society after peer review and technical editing by the publisher. To access the final edited and published work see <https://pubs.acs.org/doi/abs/10.1021/acscatal.7b01415>.

descriptor variable [*i.e.*, the magnitude of the binding between the substrate and the catalyst represented by Rxn A (Figure 1)], which subdivides each of the volcano plots (*e.g.*, Figure 2) into three areas based on its value. These three areas (defined by the descriptor variable) indicate regions in which different steps of the catalytic cycle are potential determining. Catalysts falling in region I (the “strong binding” side of the volcano) have catalyst/substrate binding interaction that are too strong, which makes reductive elimination the thermodynamically most difficult step of the catalytic cycle to complete. In contrast, catalysts in region III (the “weak binding” side of the volcano) have binding interactions that are too weak, which makes oxidative addition the thermodynamically most difficult step. In region II, the catalysts have “ideally balanced” binding energies, in line with Sabatier’s principle,^{86,87} in which case transmetalation becomes the thermodynamically most difficult process. The y-axis, on the other hand, defines the free energy need to complete the potential determining step (pds) of the catalytic cycle (*i.e.*, the most thermodynamically difficult), as defined by: $\Delta G(pds) = \max[\Delta G(Rxn A), \Delta G(Rxn B), \Delta G(Rxn C)]$. Because the y-axis plots the negative free energy of the potential determining step [- $\Delta G(pds)$], moving upward on the plot corresponds to catalysts having increasingly better thermodynamic profiles. The free energy needed to complete the potential determining step becomes progressively smaller and eventually negative (indicative of exergonicity) while moving upward on the plot. The volcano shape indicates that, in general, catalysts lying in region II, where transmetalation is the potential determining step, will have the best overall thermodynamic profiles for their specific transmetalation partners, since the - $\Delta G(pds)$ values are the smallest (least endergonic) or are negative (exergonic), depending on the specifics of the cross-coupling reaction used.

Ignoring the individual points representing specific catalysts (which will be discussed later), perhaps the most striking feature of each of the Figure 2 volcano plots is their remarkably similar shapes for the different cross-coupling protocols. This is not surprising,

This document is the Accepted Manuscript version of a Published Work that appeared in final form in ACS Catalysis, copyright © American Chemical Society after peer review and technical editing by the publisher. To access the final edited and published work see <https://pubs.acs.org/doi/abs/10.1021/acscatal.7b01415>.

however, as re-examining the catalytic cycle (Figure 1) shows that the oxidative addition and reductive elimination steps are identical for each of the six cross-coupling protocols. Their sole difference is found in the transmetallation step, which employs different cross-coupling partners, “Y”. Thus, it logically follows that differences between the transmetallation free energies are responsible for the location (*i.e.*, the height) of the volcano plateau (Figure 2). As an example, the transmetallation step in Kumada coupling involves exchanging an vinyl and a halogen on a Grignard reagent, a process that is exergonic by ~5 kcal/mol. This exergonicity translates into the transmetallation step lying toward the top of the volcano plot (area II of Figure 2b). In contrast, when silicon is used for transmetallation, as in Hiyama coupling, this step is energetically less favorable (endergonic by ~12 kcal/mol, Figure 2e) resulting in a broader plateau that is lower on the plot. Other coupling partners affect the location of the plateau in different ways (Figure 2d-f). Owing to the similarities between the volcano plots for different cross-coupling protocols it is clear that the thermodynamics of a generalized cross-coupling reaction would differ only by the location of the “volcano plateau”, which represents the free energy needed to complete transmetallation. Indeed, this exact situation is perfectly illustrated by the simulated reaction profile shown in Figure 3, in which the energetic relationship between the different Figure 2 volcano plots is established. This plot depicts the relative free energies needed to complete the transmetallation step for the six cross-coupling reactions presented in Figure 1, although any other existing or imagined transmetallation reaction could be added with another horizontal line at the corresponding free energy.

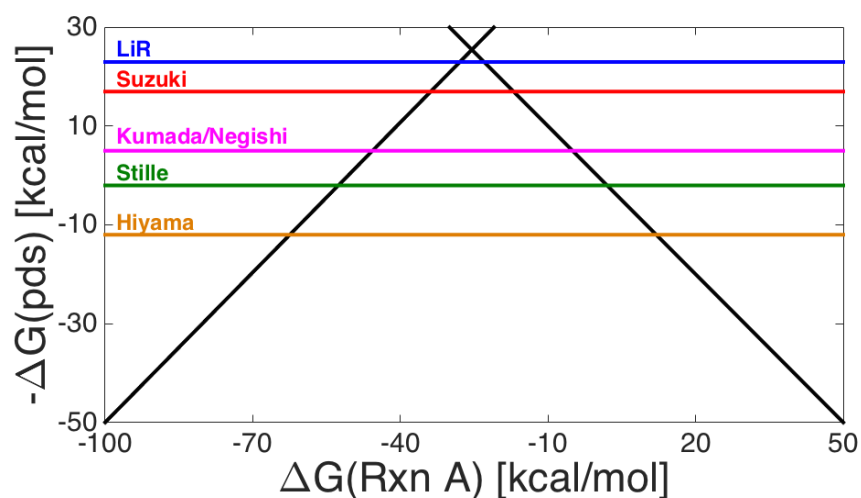


Figure 3. Simulated reaction profile showing the relationship amongst the different Figure 2 volcano plots for various cross-coupling protocols. The horizontal lines represent the free energy needed to complete the transmetalation step (Rxn B) for the six cross-coupling protocols discussed earlier, while the diagonal lines represent the free energies needed to complete reductive elimination (Rxn C, bottom left to upper right) and oxidative addition (Rxn A, bottom right to upper left).

Creating a Generalized Thermodynamic Picture. Ultimately, it would be highly desirable to create a unified cross-coupling picture capable of concisely summarizing the thermodynamics of the different “name” reactions within a single graphic.⁸⁸ As a result of the considerable similarities between the different cross-coupling protocols, this can be accomplished through construction of a 3D-volcano plot. Figure 4 depicts a schematic representation of such a plot along with a color map representation that provides a unified picture of C-C cross-coupling thermodynamics that encompasses the use of different transmetalation partners. In contrast to the typical 2D volcano plot that uses a single descriptor, this 3D variant uses two descriptor variables to explain the cross-coupling catalytic cycle. The first, $\Delta G(\text{Rxn A})$, is the same descriptor used in the 2D-volcano plots (Figure 2) and represents the magnitude of catalyst/substrate binding. The second descriptor is the free energy needed to complete the transmetalation step [$\Delta G(\text{Rxn B})$]. In choosing this particular descriptor, it becomes possible to clearly distinguish the energetic influences induced by any potential cross-coupling partner. Thus, by using two descriptors the

thermodynamics of the Figure 1 protocols can simultaneously be described and visualized, as seen in Figure 4.

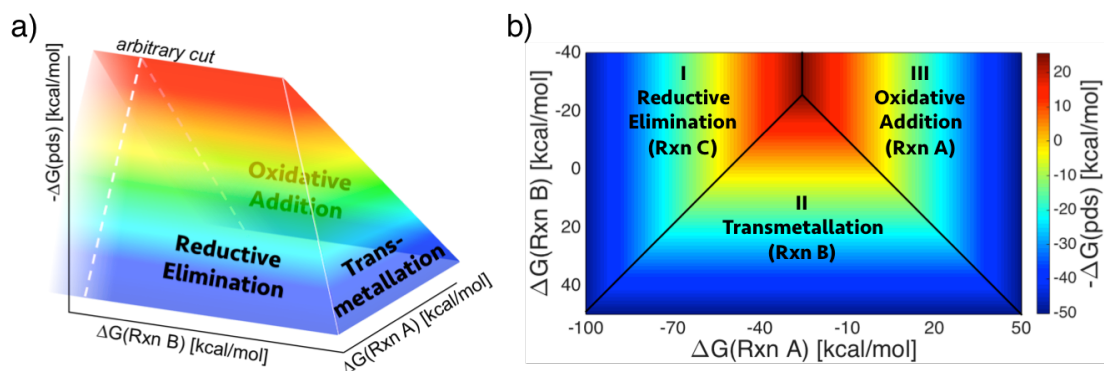


Figure 4. Two views of the 3D volcano plot describing C-C cross-coupling: a conceptualized representation (a) and a color map version (b).

As in 2D volcano plots (*e.g.*, the Figure 2 plots), the 3D volcano plot shown in Figure 4b can be divided into three sections, delineated by solid lines. The upper left and right areas represent regions in which reductive elimination and oxidative addition are the most thermodynamically difficult (potential determining) catalytic cycle steps. Comparable to 2D plots, catalysts falling into areas I and III tend to bind substrates either too strongly or too weakly, respectively. In the third region, area II, the catalytic cycle energetics are governed by the free energy needed to complete the transmetalation step. As in 2D volcano plots, catalysts lying in area II have “balanced” binding in line with Sabatier’s ideal catalyst principle.^{86,87} This means that area II of the 3D volcano plot (Figure 4b) directly corresponds to the volcano plateau in the 2D plots (Figure 2).

While gaining a comprehensive understanding of all aspects of the 3D volcano plot appears daunting, it is actually rather simple. In essence, the 3D volcano can be sliced horizontally with each slice being a unique 2D volcano plot that describes the energetics associated with using a specific cross-coupling partner for transmetalation. This point is

illustrated in Figure 5, which depicts those horizontal “slices” corresponding to the cross-coupling protocols presented in Figure 1.

The obvious conceptual advantage of 3D volcano plots is the possibility to quickly compare the energetic influence associated with using different transmetallation partners. The horizontal slices, depicted as dashed white lines in the Figure 5 color plot, clearly illustrate the considerable variation in the free energies of transmetallation. For example, Hiyama coupling (Figure 5, **F**) has the thermodynamically most difficult transmetallation step amongst the six cross-coupling protocols presented (*i.e.*, its y-axis value is the most positive). This situation contrasts organolithium (LiR) cross-coupling (Figure 5, **B**), for which the transmetallation step is highly exergonic. Such energetic factors may become of key importance when selecting a catalyst to facilitate a desired cross-coupling reaction or for the *in silico* screening on new cross-coupling catalysts (*vide infra*).

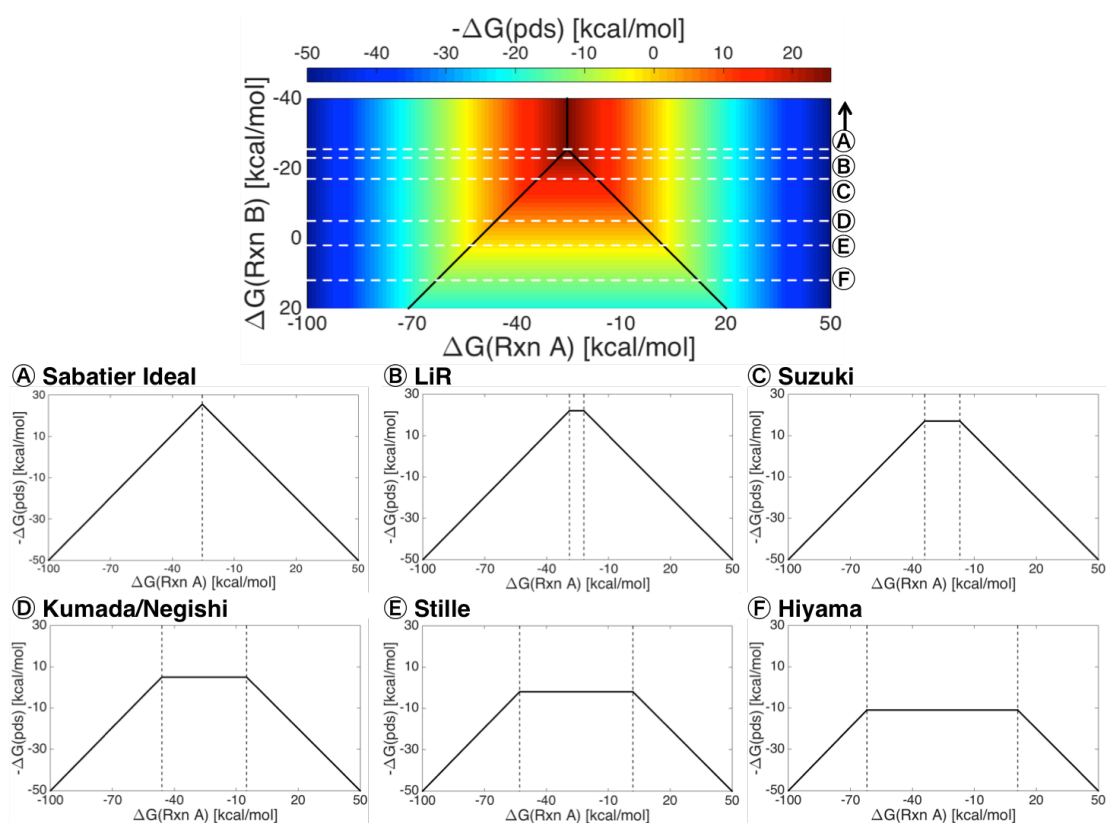


Figure 5. Relationship between 3D and 2D volcano plots. 2D horizontal “slices” perpendicular to the x,y [$\Delta G(\text{Rxn A}), \Delta G(\text{Rxn B})$] plane (**B-F**) taken from the 3D plot depict the different cross-coupling protocols described in Figure 1, as well as the “Sabatier Ideal” volcano (**A**), which has the best possible thermodynamic profile (*e.g.*, most exergonic

This document is the Accepted Manuscript version of a Published Work that appeared in final form in ACS Catalysis, copyright © American Chemical Society after peer review and technical editing by the publisher. To access the final edited and published work see <https://pubs.acs.org/doi/abs/10.1021/acscatal.7b01415>.

potential determining step) for a specific cross-coupling reaction. Note that any horizontal slices falling at $-\Delta G(\text{RxnB})$ (y-axis) values more negative than (A) each produce an identical volcano equivalent to the “Sabatier Ideal”, as indicated by the upward pointing arrow.

Despite the considerable exergonicity associated with the LiR cross-coupling protocol (~ -23 kcal/mol for the potential determining transmetallation step), in principle, the free energy needed to complete transmetallation of the catalytic cycle could be further improved by choosing an alternative cross-coupling partner. A hypothetical profile of this type is indicated by the “Sabatier ideal volcano” white dashed line (Figure 5, line A). Note that the shape of the 2D “Sabatier ideal volcano” differs from other cross-coupling reactions in that the volcano top is a summit, rather than a plateau. The appearance of this characteristic “summit” shape indicates that making the transmetallation step more exergonic no longer improves the overall thermodynamics of the catalytic cycle. Instead, the catalytic cycle thermodynamics of the “summit volcano” are dictated entirely by the free energies needed to complete either oxidative addition or reductive elimination, one of which will always be the potential determining (thermodynamically most difficult) step.

Using 3D Volcano Plots to Rationalize and Optimize Reactions. Aside from illustrating the energetic relationships between different cross-coupling protocols (Figure 5) and providing a new descriptor for screening, 3D volcano plots further provide a considerable amount of information concerning the behavior of different individual catalysts. For example, palladium phosphines have a rich and well-developed history as catalyst for cross-coupling reactions.¹⁻⁴ But why is this the case and what makes this specific metal/ligand combination so extraordinary? Figure 6 provides the answers to these questions. In short, the intrinsic properties (*i.e.*, the magnitude of the catalyst/substrate interaction) of many palladium phosphines are nearly perfectly tuned to catalyze cross-coupling reactions. In other words, these catalysts closely match Sabatier’s “ideal catalyst” for all possible cross-coupling reactions. This behavior is reflected by the vertical dashed line representing Pd(R7)₂ [denoted

“Pd”, Figure 6] which falls in the ideally balanced area (*i.e.*, the volcano top) for both Hiyama and Suzuki coupling. For the hypothetical “Sabatier ideal” cross-coupling reaction (Figure 6, A) for which the transmetalation step no longer dictates the catalytic cycle thermodynamics (*i.e.*, there is no longer a plateau atop the volcano), the palladium catalyst still lies almost directly on the volcano peak, which indicates it has nearly the best theoretically possible free energy for the catalytic cycle’s potential determining step. Thus, the 3D volcano plot predicts this palladium phosphine catalyst (and most palladium phosphine species in general) to make excellent catalysts for all cross-coupling protocols.

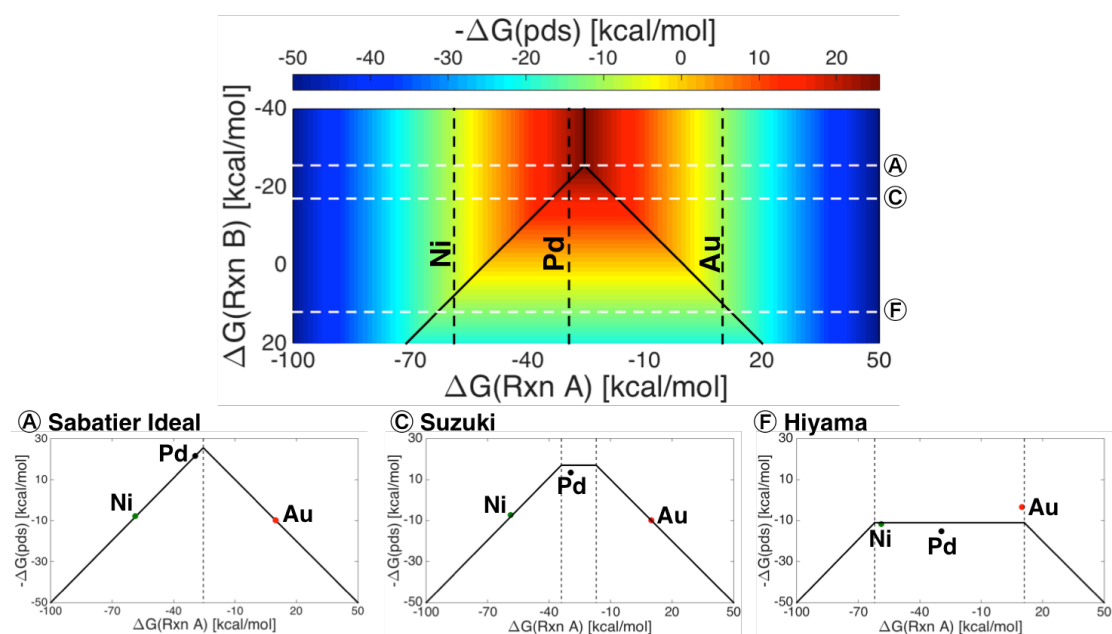


Figure 6. Relationship between the height of the volcano top and the thermodynamic profiles of different catalysts. Shifting the volcano plateau to more endergonic free energies results in an increase in the number of catalysts lying in the “ideally balanced” binding profile region (*i.e.*, between the two diagonal lines). The vertical lines represent the binding energies of specific catalysts [Ni(R7)₂, Pd(R7)₂, and Au(R7)₂], respectively. The two-dimensional volcano plots (bottom) correspond to horizontal cuts represent a Sabatier Ideal (A), as well as the Suzuki (C), and Hiyama (F) coupling protocols.

The ability of 3D volcano plots to rationalize experimentally known trends and to serve as tools for computational screening already renders them attractive for better understanding catalytic behavior. But their power is not limited to explaining experimental observations; rather, these plots also assist in reaction optimization and identifying new

This document is the Accepted Manuscript version of a Published Work that appeared in final form in ACS Catalysis, copyright © American Chemical Society after peer review and technical editing by the publisher. To access the final edited and published work see <https://pubs.acs.org/doi/abs/10.1021/acscatal.7b01415>.

catalytic species, as elegantly illustrated in Figure 6. The “Ni” vertical line represents the free energies associated with the Ni(R7)₂ catalyst, which clearly, has very different intrinsic properties than the previously discussed Pd(R7)₂ catalyst, as indicated by a catalyst/substrate binding energy difference of ~30 kcal/mol (x-axis values, Figure 6). Indeed, an assessment of the 2D “ideal” volcano (Figure 6, A) shows that this Ni species is expected to have a significantly worse thermodynamic profile than its Pd counterpart (*i.e.*, the species falls further from the volcano peak with a less exergonic potential determining step). However, by changing the transmetallation cross-coupling partners the value of the potential determining step of the Ni species become progressively closer to that of Pd. Specifically, Ni has closer energies to Pd for Suzuki coupling (Figure 6, C), while the energies of Ni are actually superior to Pd for Hiyama coupling (Figure 6, F). Similarly, broadening the volcano plateau by decreasing the exergonicity of transmetallation dramatically improves the Au(R7)₂ energetic profile relative to Pd(R7)₂. As in the Ni example, for Hiyama coupling this gold catalyst is predicted to have superior thermodynamics to its Pd counterpart.

Examples such as these highlight how 3D volcano plots provide a systematic way of identifying new catalysts through the screening of one or two easily computed descriptor variables. More generally, these plots also reveal that whether a catalyst/substrate interaction is considered “ideal” (in line with Sabatier’s principle) depends heavily on the free energies of the intermediary catalytic cycle steps (*e.g.*, transmetallation). Thus, those catalysts considered to be balanced in terms of Sabatier’s principle will vary widely depending on the specific energetics of the catalytic cycle intermediary steps. As a practical illustration of this idea, the broader plateau of Hiyama, in comparison to Suzuki, coupling (Figure 6) indicates that the former can be accomplished with a significantly more diverse set of catalysts spanning a wide-range of binding abilities [*i.e.*, the plateau spans ~70 kcal/mol along the x-axis, (Figure 6, F)], albeit with generally less desirable thermodynamics than, *e.g.*, Suzuki coupling. Thus, any catalyst having a catalyst/substrate binding energy falling within this

This document is the Accepted Manuscript version of a Published Work that appeared in final form in ACS Catalysis, copyright © American Chemical Society after peer review and technical editing by the publisher. To access the final edited and published work see <https://pubs.acs.org/doi/abs/10.1021/acscatal.7b01415>.

range is considered to be “ideally binding”. In contrast, the plateau region of the volcano for Suzuki coupling (Figure 6, C) is less broad and only spans a range of ~20 kcal/mol, meaning that far fewer catalysts will fulfill Sabatier’s “ideal binding” concept for this reaction protocol in comparison to Hiyama coupling. The opposite situation is also true, moving toward more reactive transmetallation species (*e.g.*, LiR coupling, Figure 2f) should cause the number of potential catalysts to decrease. By elegantly highlighting these relationships, 3D volcano plots not only provide an energetic overview of a chemical reaction of interest, but also reveal strategies that lead to the rational design on new chemical reactions.

Synergy between volcano plot predictions and experimental/computational findings.

A key consideration surrounding volcano plots is their ability to make predictions that match established experimental and theoretical results. Unsurprisingly, considerable effort has been placed into better understanding the mechanisms and kinetics of many types of cross-coupling reactions using a multitude of different catalysts. This include theoretical analysis of the full mechanistic cycles of Suzuki,⁸³ Negishi,⁸⁹⁻⁹² Kumada,^{93,94} and Stille⁹⁵ couplings, experimental (or combined experimental/theoretical) studies to elucidate the rate determining step,^{24,96-104} and detailed modeling of the individual oxidative addition,¹⁰⁵⁻¹⁰⁸ transmetallation,¹⁰⁹⁻¹¹⁸ and reductive elimination¹¹⁹ processes. These results largely indicate that the specific energetics of cross-coupling reactions are highly dependent upon a catalyst’s metal and ligands, the partner used for transmetallation, and the nature of the two group being coupled. Indeed, these findings are replicated in our volcano plots, where catalysts have different potential determining steps based on their specific metal/ligand combination. Assuming that Bell-Evans-Polanyi^{120,121} type relationships exist between our thermodynamic volcanoes and the kinetics of cross-coupling reactions then it would be expected that varying the metal/ligand combination of catalysts would yield different rate determining steps for the catalytic cycle. Indeed, this phenomenon is well documented in the literature. For instance, the oxidative

This document is the Accepted Manuscript version of a Published Work that appeared in final form in ACS Catalysis, copyright © American Chemical Society after peer review and technical editing by the publisher. To access the final edited and published work see <https://pubs.acs.org/doi/abs/10.1021/acscatal.7b01415>.

addition step in Suzuki coupling with Pd catalysts has long been considered to be rate-determining,⁹⁶ but transmetallation⁹⁹ and even reductive elimination⁹⁸ are rate-determining for some Suzuki coupling reactions. Similarly, the rate-determining step of Stille coupling has been experimentally assessed as being oxidative addition,²⁴ transmetallation,¹⁰⁴ or reductive elimination^{102,103} based on the specific reaction/catalyst combination. Thus, the placement of catalysts into all three volcano plot areas (Figure 2) representative of oxidative addition, transmetallation, and reductive elimination being the potential determining step, seems to match experimental observations.

Reexamining Figure 2, one striking feature that appears consistent in each of the six volcanoes is the location of many Pd based catalysts (black) along the plateau, regardless of cross-coupling partner utilized. This finding indicates that Pd species often have nearly ideal binding energies [*i.e.*, $\Delta G(\text{Rxn A})$], and, thus, are predicted to have the best thermodynamic profiles with respect to their transmetallation partners (owing to their location in region II of the Figure 2 volcano plots). Indeed, this finding aligns well with experimental assessments of the activity of palladium-based catalyst for cross-coupling reactions.¹⁻⁴

Several Pt-based catalysts also appear in region II atop each volcano, indicative of ideal binding and anticipated good catalytic activity. However, this contradicts experimental findings where Pt catalysts are virtually absent¹²² and those that do exist possess only moderate catalytic ability.¹²³ Despite this somewhat bleak outlook, some researchers have mentioned Pt as a future direction of interest.¹²⁴ The observed lack of activity of Pt catalyst, relative to their Pd counterparts, might arise from the presence of stronger M-R bonds,¹²⁵ which potentially reduces transmetallation rates. Although not observed directly in the volcano plots, our numeric results indicate that Pt catalysts have more thermodynamically favorable oxidative addition and less thermodynamically favorable reductive elimination processes than Pd catalysts (see SI Table S2-S7 for tabulated values), which aligns with previous computational results modeling reductive elimination¹²⁵⁻¹²⁷ and may contribute to

This document is the Accepted Manuscript version of a Published Work that appeared in final form in ACS Catalysis, copyright © American Chemical Society after peer review and technical editing by the publisher. To access the final edited and published work see <https://pubs.acs.org/doi/abs/10.1021/acscatal.7b01415>.

their diminished experimental capability. Thus, while Pt species are predicted to perform as well as Pd species from our volcano plots, our findings point to their problem being based on kinetics, and not thermodynamics. This situation perfectly illustrates the “best case” nature of thermodynamic volcano plots and reemphasizes their utility as preliminary screening tools for identifying catalysts that perform well.⁶⁵ Although not investigated here, a full analysis of the transition states associated with the Pt catalysts (which would normally be conducted subsequent to creating volcano plots) would likely uncover the specific reasons for their diminished performance relative to Pd catalysts.

For the coupling protocols with exergonic transmetallation steps (*e.g.*, Suzuki), Ni species appear on the strong binding side (region I), generally associated with poorer catalytic behavior than species lying on the plateau. However, manipulating the transmetallation partner to more endergonic values (*i.e.*, a downward shift of the volcano plateau) causes these species to appear on or very near the volcano top (*e.g.*, Hiyama coupling). While perhaps circumstantial in nature, it should be noted that Suzuki coupling involving Ni species was only first reported in 1997,¹²⁸ some 18 years after Pd based catalysts. In contrast, Ni and Pd catalyst for Negishi coupling were developed nearly simultaneously (Ni in 1976¹²⁹/Pd in 1977¹⁷). These findings may be related to the predicted nearly equivalent thermodynamic profiles of Ni catalysts relative to Pd for Negishi coupling [*e.g.*, Ni(S6)₂ and Pd(S6)₂, Figure 2c] and the relatively superior profiles for Pd over Ni for Suzuki coupling (Figure 2a). Of course, Ni catalysts for both Suzuki⁴⁴ and Negishi^{18,40} coupling are now relatively well developed.

Coinage metal species, in contrast to Group 10 elements, tend to be limited by the energy needed to complete the oxidative addition step and, correspondingly, generally appear on the weak binding side (region III) of the volcano. The species possessing the best thermodynamic performance still have reductive elimination values that are ~5-10 kcal/mol overall endergonic, which is roughly 20-30 kcal/mol worse than the best performing species

This document is the Accepted Manuscript version of a Published Work that appeared in final form in ACS Catalysis, copyright © American Chemical Society after peer review and technical editing by the publisher. To access the final edited and published work see <https://pubs.acs.org/doi/abs/10.1021/acscatal.7b01415>.

for Suzuki coupling (Figure 2a) but appear thermodynamically equivalent for Hiyama coupling (Figure 2e). Strides continue to be made in, for instance, C-C cross-coupling using gold catalysts¹³⁰ although the coupling may occur through an alternative mechanistic pathway¹³¹ to that studied here.

While the relative performances of catalysts incorporating different metal centers is easily deduced from the literature, establishing the change in reaction rates when different transmetallation partners are used with the same catalyst is considerably more difficult. Ideally, a series of reactions in which only the transmetallation partner was changed while all other variables (reactants, catalyst, solvent, etc.) are held constant could provide an experimental equivalent of the transmetallation free energies shown in the Figure 2 volcano plots. One noteworthy study¹³² involved the coupling of a reagent containing boron and tin termini with an aryl or alkenyl halide, which could proceed via either a Suzuki or Stille coupling process. It was found that the coupling proceeded selectively at boron and not at tin, which indicates that the thermodynamics and/or kinetics of the Suzuki coupling are more favorable than for Stille coupling. This finding aligns well with the predictions made by the 3D volcano plot, which shows that the transmetallation thermodynamics associated with Suzuki coupling is more favorable than Stille coupling.

One final outstanding question is: how do the locations of the different transmetallation partners correspond to their experimental uses? For instance, Negishi and Stille couplings are often turned to when other coupling protocols have failed, yet these appear thermodynamically less favorable than other some of the other reactions depicted in the Figure 5 3D volcano plot. It should be noted, however, that the transmetallation steps of the Negishi and Stille couplings are still exergonic (Negishi) or roughly thermoneutral (Stille), which would allow these reactions to proceed at room or slightly elevated temperatures (depending on the height of their transition state barriers). On the other hand, highly exergonic reactions, such as LiR coupling, have been reported to proceed extremely

This document is the Accepted Manuscript version of a Published Work that appeared in final form in ACS Catalysis, copyright © American Chemical Society after peer review and technical editing by the publisher. To access the final edited and published work see <https://pubs.acs.org/doi/abs/10.1021/acscatal.7b01415>.

rapidly¹³³ and may be substantially more difficult to control. This has indeed been the reputation of organolithium based cross-couplings,¹³⁴ although progress has been made to have better control over the reactions.^{35,135-138}

Conclusions

In conclusion, through the development and utilization of a 3D volcano plot we have established a generalized thermodynamic picture of C-C cross-coupling reactions. This 3D plot establishes clear links between various cross-coupling reactants and defines the energetic limit at which point varying the cross-coupling partner no longer improves the overall catalytic cycle thermodynamics. Moreover, the 3D volcano plot illustrates that the intrinsic binding properties of many Pd catalysts are ideally tuned to catalyze all types of cross-coupling reactions. Simultaneously, these plots assist in uncovering strategies for developing procedures to make less active catalysts more functional. Looking forward, we believe that 3D volcano plots represent a valuable and widely applicable tool not only for enhancing understanding of different reaction classes (as demonstrated here), but also for assisting in the identification of new homogenous catalysts based on the computation of only one or two descriptors. While this work focused on the energetic influences that accompany changing the cross-coupling partner during the transmetallation step of the catalytic cycle, in the immediate future we intend to utilize 3D volcano plots to describe other facets of different chemical reactions. Pertinent examples directly related to this work include, for example, elucidating the energetic role associated with activating cross-coupling partners, unraveling the energetic influences played by the halogen atom in oxidative addition, and determining how kinetics affect the overall picture. We reemphasize, however, that 2D and 3D volcano plots are best viewed as generally applicable tools that can be used to better understand many different chemical reactions.

This document is the Accepted Manuscript version of a Published Work that appeared in final form in ACS Catalysis, copyright © American Chemical Society after peer review and technical editing by the publisher. To access the final edited and published work see <https://pubs.acs.org/doi/abs/10.1021/acscatal.7b01415>.

Acknowledgments

The National Centre of Competence in Research (NCCR) “Materials’ Revolution: Computational Design and Discovery of Novel Materials (MARVEL)” of the Swiss National Science Foundation (SNSF) and the EPFL are acknowledged for financial support. Mr. Laurent Vannay, Dr. Ganna Gryn’ova, Prof. Jérôme Waser, and Prof. Jieping Zhu are acknowledged for technical support, helpful discussions, and critical reading of the manuscript.

References

1. *Metal-Catalyzed Cross-Coupling Reactions and More*; de Meijere, A.; Bräse, S.; Oestreich, M., Eds.; Wiley-VCH: Weinheim, 2014; Vol. 1-3.
2. *New Trends in Cross-Coupling: Theory and Applications*; Colacot, T., Ed.; The Royal Society of Chemistry: Cambridge, 2015.
3. *Applied Cross-Coupling Reactions*; Nishihara, Y., Ed.; Springer-Verlag: Berlin, 2013.
4. *Cross-Coupling and Heck-Type Reactions*; Molander, G. A., Ed.; Thieme: Stuttgart, 2013; Vol. 1.
5. Cho, S. H.; Kim, J. Y.; Kwak, J.; Chang, S. *Chem. Soc. Rev.* **2011**, *40*, 5068-5083.
6. Johansson, C. C. C.; Colacot, T. J. *Angew. Chem., Int. Ed.* **2010**, *49*, 676-707.
7. Girard, S. A.; Knauber, T.; Li, C. J. *Angew. Chem., Int. Ed.* **2014**, *53*, 74-100.
8. Rodriguez, N.; Goossen, L. J. *Chem. Soc. Rev.* **2011**, *40*, 5030-5048.
9. Xue, L.; Lin, Z. *Chem. Soc. Rev.* **2010**, *39*, 1692-1705.
10. Suzuki, A. *Angew. Chem., Int. Ed.* **2011**, *50*, 6722-6737.
11. Negishi, E. *Angew. Chem., Int. Ed.* **2011**, *50*, 6738-6764.
12. Johansson Seechurn, C. C. C.; Kitching, M. O.; Colacot, T. J.; Snieckus, V. *Angew. Chem., Int. Ed.* **2012**, *51*, 5062-5085.
13. Miyaura, N.; Yamada, K.; Suzuki, A. *Tetrahedron Lett.* **1979**, *20*, 3437-3440.
14. Miyaura, N.; Suzuki, A. *Chem. Rev.* **1995**, *95*, 2457-2483.
15. Chatterjee, A.; Ward, T. R. *Catal. Lett.* **2016**, *146*, 820-840.
16. Kotha, S.; Lahiri, K.; Kashinath, D. *Tetrahedron* **2002**, *58*, 9633-9695.
17. King, A. O.; Okukado, N.; Negishi, E. *J. Chem. Soc., Chem. Commun.* **1977**, 683-684.
18. Haas, D.; Hammann, J. M.; Greiner, R.; Knochel, P. *ACS Catal.* **2016**, *6*, 1540-1552.
19. Negishi, E. *Bull. Chem. Soc. Jpn.* **2007**, *80*, 233-257.
20. Heck, R. F.; Nolley Jr., H. P. *J. Org. Chem.* **1972**, *37*, 2320-2322.
21. McCartney, D.; Guiry, P. J. *Chem. Soc. Rev.* **2011**, *40*, 5122-5150.
22. de Meijere, A.; Meyer, F. E. *Angew. Chem., Int. Ed.* **1995**, *33*, 2379-2411.
23. Milstein, D.; Stille, J. K. *J. Am. Chem. Soc.* **1978**, *100*, 3636-3638.
24. Milstein, D.; Stille, J. K. *J. Am. Chem. Soc.* **1979**, *101*, 4992-4998.
25. Milstein, D.; Stille, J. K. *J. Org. Chem.* **1979**, *44*, 1613-1618.
26. Cordovilla, C.; Bartolomé, C.; Martínez-Illarduya, J. M.; Espinet, P. *ACS Catal.* **2015**, *5*, 3040-3053.
27. Hatanaka, Y.; Hiyama, T. *J. Org. Chem.* **1988**, *53*, 918-920.
28. Nakao, Y.; Hiyama, T. *Chem. Soc. Rev.* **2011**, *40*, 4893-4901.
29. Sore, H. F.; Galloway, W. R. J. D.; Spring, D. R. *Chem. Soc. Rev.* **2012**, *41*, 1845-1866.
30. Tamao, K.; Sumitani, K.; Kumada, M. *J. Am. Chem. Soc.* **1972**, *94*, 4374-4376.
31. Corriu, R. J. P.; Masse, J. P. *J. Chem. Soc., Chem. Commun.* **1972**, 144a.
32. Knappke, C. E. I.; Jacobi von Wangelin, A. *Chem. Soc. Rev.* **2011**, *40*, 4948-4962.
33. Tamura, M.; Kochi, J. K. *J. Am. Chem. Soc.* **1971**, *93*, 1487-1489.
34. Smith, R. S.; Kochi, J. K. *J. Org. Chem.* **1976**, *41*, 502-509.

This document is the Accepted Manuscript version of a Published Work that appeared in final form in ACS Catalysis, copyright © American Chemical Society after peer review and technical editing by the publisher. To access the final edited and published work see <https://pubs.acs.org/doi/abs/10.1021/acscatal.7b01415>.

35. Giannerini, M.; Fañanás-Mastral, M.; Feringa, B. L. *Nat. Chem.* **2013**, *5*, 667-672.
36. *Ni- and Fe- Based Cross-Coupling Reactions*; Correa, A., Ed.; Springer International Publishing, 2016; Vol. 374.
37. Zhou, J.; Fu, G. C. *J. Am. Chem. Soc.* **2003**, *125*, 14726-14727.
38. Zhou, J.; Fu, G. C. *J. Am. Chem. Soc.* **2004**, *126*, 1340-1341.
39. Sherry, B. D.; Fürstner, A. *Acc. Chem. Res.* **2008**, *41*, 1500-1511.
40. Phapale, V. B.; Cárdenas, D. J. *Chem. Soc. Rev.* **2009**, *38*, 1598-1607.
41. Hu, X. *Chem. Sci.* **2011**, *2*, 1867-1886.
42. Jana, R.; Pathak, T. P.; Sigman, M. S. *Chem. Rev.* **2011**, *111*, 1417-1492.
43. Mesganaw, T.; Garg, N. K. *Org. Process Res. Dev.* **2013**, *17*, 29-39.
44. Han, F.-S. *Chem. Soc. Rev.* **2013**, *42*, 5270-5298.
45. Tasker, S. Z.; Standley, E. A.; Jamison, T. F. *Nature* **2014**, *509*, 299-309.
46. Bedford, R. B. *Acc. Chem. Res.* **2015**, *48*, 1485-1493.
47. Bauer, I.; Knölker, H.-J. *Chem. Rev.* **2015**, *115*, 3170-3387.
48. Kuzmina, O. M.; Steib, A. K.; Moyeux, A.; Cahiez, G.; Knochel, P. *Synthesis* **2015**, *47*, 1696-1705.
49. Cassani, C.; Bergonzini, G.; Wallentin, C.-J. *ACS Catal.* **2016**, *6*, 1640-1648.
50. Martin, R.; Buchwald, S. L. *Acc. Chem. Res.* **2008**, *41*, 1561-1473.
51. Barder, T. E.; Walker, S. D.; Martinelli, J. R.; Buchwald, S. L. *J. Am. Chem. Soc.* **2005**, *127*, 4685-4696.
52. Jover, J.; Fey, N.; Purdie, M.; Lloyd-Jones, G. C.; Harvey, J. N. *J. Mol. Catal. A* **2010**, *324*, 39-47.
53. Fihri, A.; Meunier, P.; Hierso, J.-C. *Coord. Chem. Rev.* **2007**, *251*, 2017-2055.
54. Miura, M. *Angew. Chem., Int. Ed.* **2004**, *43*, 2201-2203.
55. Surry, D. S.; Buchwald, S. L. *Angew. Chem., Int. Ed.* **2008**, *47*, 6338-6361.
56. Fu, G. C. *Acc. Chem. Res.* **2008**, *41*, 1555-1564.
57. Birkholz, M.-N.; Freixa, Z.; van Leeuwen, P. W. N. M. *Chem. Soc. Rev.* **2009**, *38*, 1099-1118.
58. Valente, C.; Çalimsiz, S.; Hoi, K. H.; Mallik, D.; Sayah, M.; Organ, M. G. *Angew. Chem., Int. Ed.* **2012**, *51*, 3314-3332.
59. Kantchev, E. A. B.; O'Brien, C. J.; Organ, M. G. *Angew. Chem., Int. Ed.* **2007**, *46*, 2768-2813.
60. Gerischer, H. *Bull. Soc. Chim. Belg.* **1958**, *67*, 506-527.
61. Parsons, R. *Trans. Faraday Soc.* **1958**, *54*, 1053-1063.
62. Nørskov, J. K.; Bligaard, T.; Rossmeisl, J.; Christensen, C. H. *Nat. Chem.* **2009**, *1*, 37-46.
63. Dau, H.; Limberg, C.; Reier, T.; Risch, M.; Roggan, S.; Strasser, P. *ChemCatChem* **2010**, *2*, 724-761.
64. Greeley, J.; Markovic, N. M. *Energy Environ. Sci.* **2012**, *5*, 9246-9256.
65. Busch, M.; Wodrich, M. D.; Corminboeuf, C. *Chem. Sci.* **2015**, *6*, 6754-6761.
66. Wodrich, M. D.; Busch, M.; Corminboeuf, C. *Chem. Sci.* **2016**, *7*, 5723-5735.
67. del Pozo, J.; Pérez-Iglesias, M.; Álvarez, R.; Lledós, A.; Casares, J. A.; Espinet, P. *ACS Catal.* **2017**, *7*, 3575-3583.
68. Cheng, J.; Hu, P. *J. Am. Chem. Soc.* **2008**, *130*, 10868-10869.
69. Andersen, M.; Medford, A. J.; Nørskov, J. K.; Reuter, K. *Angew. Chem., Int. Ed.* **2016**, *55*, 5210-5214.
70. Technical problems prevented the computation of several Cu species.
71. The nature of the ligation state of the catalysts is an important issue of which we are keenly aware. Work is currently underway in our laboratory on ways to treat differences in ligation state and how best to incorporate this information into volcano plots.
72. Miyaura, N. *Top. Curr. Chem.* **2002**, *219*, 11-59.
73. Brill, W. K.-D.; Papeo, G. In *Combinatorial Chemistry: From Theory to Application, Volume 26*; Bannwarth, W., Hinzen, B., Eds.; Wiley-VCH: Weinheim, 2006, p 143-360.
74. Zhao, Y.; Truhlar, D. G. *Acc. Chem. Res.* **2008**, *41*, 157-167.
75. Zhao, Y.; Truhlar, D. G. *Theor. Chem. Acc.* **2008**, *120*, 215-241.
76. Weigend, F.; Ahlrichs, R. *Phys. Chem. Chem. Phys.* **2005**, *7*, 3297-3305.
77. Marenich, A. V.; Cramer, C. J.; Truhlar, D. G. *J. Phys. Chem. B* **2009**, *113*, 4775-4777.
78. Frisch, M. J.; Trucks, G. W.; Schlegel, H. B.; Scuseria, G. E.; Robb, M. A.; Cheeseman, J. R.; Scalmani, G.; Barone, V.; Mennucci, B.; Petersson, G. A.; Nakatsuji, H.; Caricato, M.; Li, X.; Hratchian, H. P.; Izmaylov, A. F.; Bloino, J.; Zheng, G.; Sonnenberg, J. L.; Hada, M.; Ehara, M.; Toyota, K.; Fukuda, R.; Hasegawa, J.; Ishida, M.; Nakajima, T.; Honda, Y.; Kitao, O.; Nakai, H.;

This document is the Accepted Manuscript version of a Published Work that appeared in final form in ACS Catalysis, copyright © American Chemical Society after peer review and technical editing by the publisher. To access the final edited and published work see <https://pubs.acs.org/doi/abs/10.1021/acscatal.7b01415>.

Vreven, T.; Montgomery, J. A.; Peralta, J. E.; Ogliaro, F.; Bearpark, M.; Heyd, J. J.; Brothers, E.; Kudin, K. N.; Staroverov, V. N.; Kobayashi, R.; Normand, J.; Raghavachari, K.; Rendell, A.; Burant, J. C.; Iyengar, S. S.; Tomasi, J.; Cossi, M.; Rega, N.; Millam, M. J.; Klene, M.; Knox, J. E.; Cross, J. B.; Bakken, V.; Adamo, C.; Jaramillo, J.; Gomperts, R.; Stratmann, R. E.; Yazyev, O.; Austin, A. J.; Cammi, R.; Pomelli, C.; Ochterski, J. W.; Martin, R. L.; Morokuma, K.; Zakrzewski, V. G.; Voth, G. A.; Salvador, P.; Dannenberg, J. J.; Dapprich, S.; Daniels, A. D.; Farkas, O.; Foresman, J. B.; Ortiz, J. V.; Cioslowski, J.; Fox, D. J.; Gaussian, Inc.: Wallingford, CT, 2009.

79. Wheeler, S. E.; Houk, K. N. *J. Chem. Theory Comput.* **2010**, *6*, 395-404.
80. Tamura, H.; Yamazaki, H.; Sato, H.; Sakaki, S. *J. Am. Chem. Soc.* **2003**, *125*, 16114-16126.
81. Sakaki, S.; Takayama, T.; Sumimoto, M.; Sugimoto, M. *J. Am. Chem. Soc.* **2004**, *126*, 3332-3348.
82. Sumimoto, M.; Iwane, N.; Takhama, T.; Sakaki, S. *J. Am. Chem. Soc.* **2004**, *126*, 10457-10471.
83. Braga, A. A. C.; Ujaque, G.; Maseras, F. *Organometallics* **2006**, *25*, 3647-3658.
84. Amatore, C.; Jutand, A.; Le Duc, G. *Chem. - Eur. J.* **2011**, *17*, 2492-2503.
85. Amatore, C.; Le Duc, G.; Jutand, A. *Chem. - Eur. J.* **2013**, *19*, 10082-10093.
86. Sabatier, P. *Ber. Deutsch. Chem. Gesellschaft* **1911**, *44*, 1984-2001.
87. Sabatier, P. *La Catalyse en Chimie Organique*; Librairie Polytechnique: Paris, 1913.
88. The generalized picture also would be able to describe the cross-coupling reaction with any existing or hypothetical transmetallation partner. Here, however, only the six named reactions given in Figure 1 are considered.
89. Lin, X.; Phillips, D. L. *J. Org. Chem.* **2008**, *73*, 3680-3688.
90. González-Pérez, A. B.; Álvarez, R.; Nito Faza, O.; de Lera, Á. R.; Aurrecochea, J. M. *Organometallics* **2012**, *31*, 2053-2058.
91. Chass, G. A.; O'Brien, C. J.; Hadei, N.; Kantchev, E. A. B.; Mu, W.-H.; Fang, D.-C.; Hopkinson, A. C.; Csizmadia, I. G.; Organ, M. G. *Chem. - Eur. J.* **2009**, *15*, 4281-4288.
92. Phapale, V. B.; Guisán-Ceinos, M.; Buñuel, E.; Cárdenas, D. J. *Chem. - Eur. J.* **2009**, *15*, 12681-12688.
93. Ogawa, H.; Minami, H.; Ozaki, T.; Komagawa, S.; Wang, C.; Uchiyama, M. *Chem. - Eur. J.* **2015**, *21*, 13904-13908.
94. Kleimark, J.; Hedström, A.; Larsson, P.-F.; Jahansson, C.; Norrby, P.-O. *ChemCatChem* **2009**, *1*, 152-161.
95. Álvarez, R.; Faza, O. N.; López, C. S.; de Lera, Á. R. *Org. Lett.* **2006**, *8*, 35-38.
96. Smith, G. B.; Dezeny, G. C.; Hughes, D. L.; King, A. O.; Verhoeven, T. R. *J. Org. Chem.* **1994**, *59*, 8151-8156.
97. Molander, G. A.; Shin, I. *Org. Lett.* **2011**, *13*, 3956-3959.
98. He, X.; Zhang, S.; Guo, Y.; Wang, H.; Lin, G. *Organometallics* **2012**, *31*, 2945-2948.
99. Dufert, M. A.; Billingsley, K. L.; Buchwald, S. L. *J. Am. Chem. Soc.* **2013**, *135*, 12877-12885.
100. Jin, L.; Xin, J.; Huang, Z.; He, J.; Lei, A. *J. Am. Chem. Soc.* **2010**, *132*, 9607-9609.
101. Li, J.; Jin, L.; Liu, C.; Lei, A. *Org. Chem. Front.* **2014**, *1*, 50-53.
102. Goliaszewski, A.; Schwartz, J. *J. Am. Chem. Soc.* **1984**, *106*, 5028-5030.
103. Goliaszewski, A.; Schwartz, J. *Organometallics* **1985**, *4*, 417-419.
104. Espinet, P.; Echavarren, A. M. *Angew. Chem., Int. Ed.* **2004**, *43*, 4704-4734.
105. Goossen, L. J.; Koley, D.; Hermann, H. L.; Thiel, W. *Chem. Commun.* **2004**, 2141-2143.
106. Goossen, L. J.; Koley, D.; Hermann, H. L.; Thiel, W. *Organometallics* **2005**, *24*, 2398-2410.
107. Lam, K. C.; Marder, T. B.; Lin, Z. *Organometallics* **2007**, *26*, 758-760.
108. McMullin, C. L.; Jover, J.; Harvey, J. N.; Fey, N. *Dalton Trans.* **2010**, *39*, 10833-10836.
109. Braga, A. A. C.; Morgon, N. H.; Ujaque, G.; Lledós, A.; Maseras, F. *J. Organomet. Chem.* **2006**, *691*, 4459-4466.
110. Sicre, C.; Braga, A. A. C.; Maseras, F.; Cid, M. M. *Tetrahedron* **2008**, *64*, 7437-7443.
111. Braga, A. A. C.; Morgon, N. H.; Ujaque, G.; Maseras, F. *J. Am. Chem. Soc.* **2005**, *127*, 9298-9307.
112. Weng, C.-M.; Hong, F.-E. *Dalton Trans.* **2011**, *40*, 6458-6468.
113. Ortuño, M. A.; Lledós, A.; Maseras, F.; Ujaque, G. *ChemCatChem* **2014**, *6*, 3132-3138.
114. Fuentes, B.; García-Melchor, M.; Lledós, A.; Maseras, F.; Casares, J. A.; Ujaque, G.; Espinet, P. *Chem. - Eur. J.* **2010**, *16*, 8596-8599.
115. del Pozo, J.; Salas, G.; Álvarez, R.; Casares, J. A.; Espinet, P. *Organometallics* **2016**, *35*, 3604-3611.

This document is the Accepted Manuscript version of a Published Work that appeared in final form in ACS Catalysis, copyright © American Chemical Society after peer review and technical editing by the publisher. To access the final edited and published work see <https://pubs.acs.org/doi/abs/10.1021/acscatal.7b01415>.

116. Nova, A.; Ujaque, G.; Maseras, F.; Lledós, A.; Espinet, P. *J. Am. Chem. Soc.* **2006**, *128*, 14571-14578.
117. Álvarez, R.; Pérez, M.; Faza, O. N.; de Lera, A. R. *Organometallics* **2008**, *27*, 3378-3389.
118. Cheng, K.; Wang, C.; Ding, Y.; Song, Q.; Qi, C.; Zhang, X.-M. *J. Org. Chem.* **2011**, *76*, 9261-9268.
119. Pérez-Rodríguez, M.; Braga, A. A. C.; Garcia-Melchor, M.; Pérez-Temprano, M. H.; Casares, J. A.; Ujaque, G.; de Lera, A. R.; Álvarez, R.; Maseras, F.; Espinet, P. *J. Am. Chem. Soc.* **2009**, *131*, 3650-3657.
120. Bell, R. P. *Proc. R. Soc. London, Ser. A* **1936**, *154*, 414-429.
121. Evans, D. J.; Polanyi, M. *Trans. Faraday Soc.* **1938**, *34*, 11-24.
122. Bedford, R. B.; Hazelwood, S. L.; Albisson, D. A. *Organometallics* **2002**, *21*, 2599-2600.
123. Mateo, C.; Fernández-Rivas, C.; Cárdenas, D. J.; Echavarren, A. M. *Organometallics* **1998**, *17*, 3661-3669.
124. Adhikary, A.; Guan, H. *ACS Catal.* **2015**, *5*, 6858-6873.
125. Ananikov, V. P.; Musaev, D. G.; Morokuma, K. *Organometallics* **2005**, *24*, 715-723.
126. Low, J. J.; Goddard III, W. A. *Organometallics* **1985**, *5*, 609-622.
127. Low, J. J.; Goddard III, W. A. *J. Am. Chem. Soc.* **1986**, *108*, 6115-6128.
128. Saito, S.; Oh-tani, S.; Miyaura, N. *J. Org. Chem.* **1997**, *62*, 8024-8030.
129. Negishi, E.; Baba, S. *J. Chem. Soc., Chem. Commun.* **1976**, 596b-597b.
130. Garcia, P.; Malacria, M.; Aubert, C.; Gandon, V.; Fensterbank, L. *ChemCatChem* **2010**, *2*, 493-497.
131. Zhang, G.; Peng, Y.; Cui, L.; Zhang, L. *Angew. Chem., Int. Ed.* **2009**, *48*, 3112-3115.
132. Ishiyama, T.; Miyaura, N.; Suzuki, A. *Synlett* **1991**, 687-688.
133. Nagaki, A.; Kenmoku, A.; Moriwaki, Y.; Hayashi, A.; Yoshida, J. *Angew. Chem., Int. Ed.* **2010**, *49*, 7543-7547.
134. Firth, J. D.; O'Brien, P. *ChemCatChem* **2015**, *7*, 395-397.
135. Hornillos, V.; Giannerini, M.; Vila, C.; Fañanás-Mastral, M.; Feringa, B. L. *Org. Lett.* **2013**, *15*, 5114-5117.
136. Vila, C.; Hornillos, V.; Giannerini, M.; Fañanás-Mastral, M.; Feringa, B. L. *Chem. - Eur. J.* **2014**, *20*, 13078-13083.
137. Vila, C.; Giannerini, M.; Hornillos, V.; Fañanás-Mastral, M.; Feringa, B. L. *Chem. Sci.* **2014**, *5*, 1361-1367.
138. Giannerini, M.; Hornillos, V.; Vila, C.; Fañanás-Mastral, M.; Feringa, B. L. *Angew. Chem., Int. Ed.* **2013**, *52*, 13329-13333.

TOC Graphic:

